

UNCLASSIFIED



Australian Government

Department of Defence

Defence Science and
Technology Group

Deflection and Supporting Force Analysis of a Slender Beam under Combined Transverse and Tensile Axial Loads

Witold Waldman and Xiaobo Yu

Aerospace Division

Defence Science and Technology Group

DST-Group-TR-3254

ABSTRACT

This report describes the deflection and supporting force analysis of a static pressure pipe that is to be used in the Defence Science and Technology Group Transonic Wind Tunnel test facility. The static pressure pipe was modelled as a slender propped cantilever beam (fixed at one end and roller-supported at the other) that is subjected to combined transverse and tensile axial loading. An analytical solution to this problem has been derived from first principles using Euler-Bernoulli beam theory, and a closed-form expression for the beam deflection as a function of the axial tension force is provided. The analytical solution was checked by performing a separate nonlinear finite element analysis using beam elements. The value of the peak deflection and its position along the beam axis was determined as a function of the applied axial tension force by solving a nonlinear equation using the bisection method. The analytical functions and numerical solution methods described in this report have been implemented for general use in a spreadsheet, and the source code for these is provided. They can be used to study other slender beam configurations that may be of interest. A modal finite element analysis of a further idealised beam configuration was also conducted to provide estimates of the natural frequencies and associated mode shapes for the beam.

RELEASE LIMITATION

Approved for public release

UNCLASSIFIED

UNCLASSIFIED

Published by

*Aerospace Division
Defence Science and Technology Group
506 Lorimer Street
Fishermans Bend, Victoria 3207, Australia*

*Telephone: 1300 333 362
Fax: (03) 9626 7999*

*© Commonwealth of Australia 2016
AR-016-592
May 2016*

APPROVED FOR PUBLIC RELEASE

UNCLASSIFIED

UNCLASSIFIED

Deflection and Supporting Force Analysis of a Slender Beam under Combined Transverse and Tensile Axial Loads

Executive Summary

Aerospace Division has been deeply involved in the development and application of technologies that help to ensure the safety and enhance the availability of aircraft in service with the Royal Australian Air Force. The Flight and Fluid Dynamics Group in the Aircraft Performance and Survivability Branch undertakes research into steady and unsteady fluid dynamics in incompressible, subsonic, transonic, supersonic and hypersonic flow. This is applied to studies involving fixed wing flight vehicles, submarines and surface vessels, aeroelastic and structural dynamic behaviour, flight dynamic behaviour and performance, as well as weapon aerodynamics and integration.

This report details the deflection and supporting force analysis relating to the design of a static pressure pipe that is to be used in the Defence Science and Technology Group Transonic Wind Tunnel test facility. The static pressure pipe analysed herein was modelled as a slender propped cantilever beam (fixed at one end and roller-supported at the other) that is subjected to combined transverse and tensile axial loading. Although an analytical solution to this beam problem is available for the limiting case of zero axial tension force, a published solution for the case of general non-zero tension loading could not be found, even though a number of engineering handbooks were consulted.

For the present problem, that of a slender propped cantilever beam subjected to combined transverse and tensile axial loading, the work documented in this report has resulted in the derivation of a new analytical solution that is applicable to this particular beam geometry and loading. The solution is based on the application of the well-known Euler-Bernoulli beam theory to this problem. The key result is a compact closed-form expression for the beam deflection as a function of the axial tension force. The value of the peak deflection and its position along the beam axis were also determined as a function of the applied axial tension force, by solving a nonlinear equation using the bisection method. The analytical functions and numerical solution methods described in this report have been implemented for general use in a spreadsheet, and the associated source code is provided. A modal analysis of an idealised version of the beam to determine its natural frequencies and mode shapes has also been conducted in order to gain some insight into the flexural vibration characteristics of this structure.

UNCLASSIFIED

Authors

Witold Waldman

Aerospace Division

Mr Witold Waldman completed a BEng (with distinction) in Aeronautical Engineering at the Royal Melbourne Institute of Technology in 1981. He commenced work in Structures Division in 1982 at what was then the Aeronautical Research Laboratory. He has published a number of papers and reports, and his experience has focussed on stress analysis using finite element and boundary element methods, structural mechanics, fracture mechanics, computational unsteady aerodynamics, structural dynamics testing, digital filtering of flight test data, nonlinear optimisation, and spectral analysis. His recent work has been in the areas of structural shape optimisation and computation of stress intensity factors. He is currently a Senior Research Engineer in the Structural and Damage Mechanics Group in the Airframe Technology and Safety Branch of Aerospace Division within the Defence Science and Technology Group, Department of Defence.

Xiaobo Yu

Aerospace Division

Xiaobo Yu completed a BEng in Naval Architecture Engineering in 1988, and a MEng in Structural Mechanics in 1991, both from Shanghai Jiao Tong University, and a PhD in Civil Engineering from the University of Sydney. He has held a lecturing position in Shanghai Jiao Tong University and several senior research positions in the University of Sydney and the University of NSW, and was also attached to Pacific Engineering Systems International as a CRC-ACS visiting research fellow. He joined what was then the Defence Science and Technology Organisation in 2007, and is currently Science Team Leader for Structural Mechanics in Aerospace Division. His main interests and responsibilities include: structural shape optimisation, computational structural analysis and multi-axial fatigue, in the context of airframe safety and life assessment and life extension.

Contents

1. INTRODUCTION.....	1
2. BEAM GEOMETRY AND MATERIAL PROPERTIES	1
3. STATIC ANALYSIS	2
3.1 Analytical solution for tension force $T = 0$ case (textbook).....	2
3.2 Analytical solution for tension force $T > 0$ case (this study).....	3
3.3 Nonlinear FEA solution for tension force $T \geq 0$ case.....	6
3.4 Computed analytical and nonlinear FEA results	6
4. DYNAMIC ANALYSIS.....	8
4.1 Analytical modal solution for tension force $T = 0$ case (textbook).....	8
4.2 Computed nonlinear FEA results for tension force $T \geq 0$ case (this study)	9
4.3 Empirical formula for calculation of beam natural frequency for $T \geq 0$ case (this study)	10
4.4 Calculation of cable natural frequency for $T \geq 0$ case (textbook)	11
5. CONCLUSIONS.....	12
6. REFERENCES	13
APPENDIX A: LISTING OF SYMPY SYMBOLIC COMPUTATIONS	25
APPENDIX B: VBA FUNCTIONS FOR STATIC SOLUTION OF PROPPED CANTILEVER BEAM SUBJECTED TO COMBINED TRANSVERSE AND AXIAL LOADING	27

Nomenclature

a, b, c, d	coefficients in nonlinear beam deflection equation
A	cross-sectional area
dv/dx	first derivative of beam displacement with respect to x
d^2v/dx^2	second derivative of beam displacement with respect to x
E	Young's modulus
f_n	n^{th} natural frequency of flexural transverse vibration
f_{cn}	n^{th} natural frequency cable transverse vibration
g	acceleration due to gravity
I	second moment of area about centroid
k	$\sqrt{\frac{T}{EI}}$
L	length of beam
m	total mass of pipe or beam
$M(x)$	bending moment
M_e	reaction moment at encastre end of beam
n	order of natural vibration mode
$q(x)$	transverse loading
R_e	vertical reaction force at encastre end of beam
R_p	vertical reaction force at propped end of beam
t	wall thickness of static pressure pipe
T	applied axial tension force
T_c	applied cable tension force
$v(x)$	transverse deflection of beam
$V(x)$	shear force
W	weight per unit length
x	distance along horizontal axis
$x_{\delta_{max}}$	position of point of maximum deflection of beam
y	distance along vertical axis
α_n, β_n	parameters in vibration mode shape equation
δ_{max}	maximum deflection of beam
ξ_n	parameter in natural frequency equation
κ	curvature
Φ_i	internal diameter of pipe
Φ_o	external diameter of pipe
ψ_n	n^{th} characteristic mode shape
θ_p	angle of rotation of propped end of beam
Υ	volume
ρ	density
μ_c	mass per unit length of cable

1. Introduction

This report documents an analysis of a slender beam under combined transverse and tensile axial loads. The analysis was primarily performed to determine the maximum static deflection of a static pressure pipe that is to be used during aerodynamic testing work conducted in the Defence Science and Technology Group Transonic Wind Tunnel facility. A layout diagram of the static pressure pipe installation is shown in Figure 1 (as supplied by the Aerodynamics and Aeroelasticity Group).

For the purpose of the analysis, the static pressure pipe was modelled as a slender propped cantilever beam, fixed at one end and roller-supported at the other, as shown in Figure 2. The transverse load $q(x)$ is the uniform self-weight loading distributed along the length of the beam, and T is the axial tension force. The analysis was performed to provide solutions to:

- (i) the maximum deflection of the beam,
- (ii) the position of the maximum deflection, and
- (iii) the value of the supporting force R_p at the propped end of the beam.

The forces T and R_p represent the horizontal and vertical components of the vector summation of the cable pulling forces applied at the right-hand side of the beam as depicted in Figure 1.

It is noted here that the solutions as mentioned above for tensile forces $T > 0$ are not available in textbooks or handbooks. Nor can they be obtained using linear finite element analysis (FEA), a general-purpose computational tool whose reliability in performing such analyses is known to the Structural and Damage Mechanics Group in Aerospace Division. As such, in the present study, an analytical solution for the $T > 0$ case was derived from first principles based on Euler-Bernoulli beam theory [1]. Then, a nonlinear FEA using beam elements was performed for the purpose of checking the deflection computed using the analytical equation. A modal analysis of the beam has also been conducted to determine its natural frequencies and associated mode shapes in order to gain some insight into the flexural vibration characteristics of this structure.

Section 2 describes the general beam geometry and defines the material properties used in the analysis work. The analytical and nonlinear FEA solutions for the static deflection of a propped cantilever beam problem for axial tension forces $T \geq 0$ are presented in Section 3. The results of a dynamic nonlinear FEA modal response analysis for $T \geq 0$ are presented in Section 4, together with an analytical solution for the $T = 0$ case. Finally, the conclusions are provided in Section 5.

2. Beam geometry and material properties

The beam that is being analysed here has a length of $L = 4500$ mm. It consists of a uniform circular pipe with a wall thickness $t = 3.0$ mm, whose outside diameter is $\varnothing_o = 38.1$ mm and the inside diameter is $\varnothing_i = 32.1$ mm. The cross-sectional area of the pipe is then

calculated to be $A = \pi(\phi_o^2 - \phi_i^2)/4 = 330.81 \text{ mm}^2$, and the total volume of the beam is $Y = LA = 1.4886 \times 10^6 \text{ mm}^3$. The second moment of area of the beam about the horizontal axis passing through the centroid of the cross-section is $I = \pi(\phi_o^4 - \phi_i^4)/64 = 51317 \text{ mm}^4$.

The pipe is manufactured from a steel material, whose Young's modulus is assumed to be $E = 200 \times 10^3 \text{ N/mm}^2$. The density of the steel is assumed to be $\rho = 7.850 \times 10^{-6} \text{ kg/mm}^3$. Thus the total mass of the beam is $m = \rho Y = 11.686 \text{ kg}$. The weight of the beam per unit length is calculated to be $W = mg/L = 2.5468 \times 10^{-2} \text{ N/mm}$, where the acceleration due to gravity is taken to be $g = 9.807 \text{ m/s}^2$. It is noted here that the mass contribution of the pressure measurement tubing that will be installed inside the pipe has not been included.

3. Static analysis

Referring to Figure 2, the beam that represents the static pressure pipe has an encastre support (also commonly referred to as a fixed or clamped support) at the left-hand end, and it can neither translate nor rotate. At the propped end, the beam is free to rotate (roller support) as well as translate in the x -direction, but it is restrained from motion in the y -direction.

In determining the static deflection, it will be assumed that classical Euler-Bernoulli beam theory applies [1]. Here this means that it is assumed that: (i) the beam cross-section does not deform in its plane or warp out of its plane, and that this cross-sectional plane remains normal to the beam axis; and (ii) the deformation of the beam is dominated by bending. These assumptions are applicable to slender beams, a category to which the present beam belongs, as its cross-sectional diameter is much smaller than its length ($\phi_o/L = 0.0085 \cong 0$).

3.1 Analytical solution for tension force $T = 0$ case (textbook)

Amongst many other example problems, Gere and Timoshenko [2] have analysed the statically-indeterminate propped cantilever beam shown in Figure 2 for the case of zero tension force, $T = 0$, and a uniform transverse loading of intensity $q(x) = W$. They have described the solution in their Example 10-1 found in [2]. There they have derived closed-form equations for the shear force distribution $V(x)$, the bending moment distribution $M(x)$, the deflection shape $v(x)$, the slope along the beam dv/dx , the curvature along the beam d^2v/dx^2 , the maximum deflection δ_{max} of the beam, the x -location of the maximum deflection $x_{\delta_{max}}$, the angle of rotation at the propped end of the beam θ_p , the vertical reaction force at the propped end R_p , the vertical reaction force at the encastre end R_e , and the reaction moment at the encastre end M_e . The relevant formulae are provided in Equations (1)-(10) below.

$$V(x) = \frac{1}{8}(5L - 8x)W \quad (1)$$

$$M(x) = \frac{1}{8}(-L^2 + 5Lx - 4Lx^2)W \quad (2)$$

$$v(x) = -\frac{1}{48EI}(3L^2x^2 - 5Lx^3 + 2x^4)W \quad (3)$$

$$\frac{dv}{dx} = -\frac{1}{48EI} (6L^2x - 15Lx^2 + 8x^3) W \quad (4)$$

$$\frac{d^2v}{dx^2} = -\frac{1}{48EI} (6L^2 - 30Lx + 24x^2) W \quad (5)$$

$$\delta_{max} = -(v)_{x=x_{\delta max}} = \frac{(39+55\sqrt{33})}{65536 EI} WL^4 \quad \text{at} \quad x_{\delta max} = \frac{15-\sqrt{33}}{16} L \quad (6)$$

$$\theta_p = \left(\frac{dv}{dx}\right)_{x=L} = \text{atan}\left(\frac{1}{48EI} WL^3\right) \quad (7)$$

$$R_p = \frac{3}{8} WL \quad (8)$$

$$R_e = \frac{5}{8} WL \quad (9)$$

$$M_e = \frac{1}{8} WL^2 \quad (10)$$

3.2 Analytical solution for tension force $T > 0$ case (this study)

Consider an infinitesimally small segment of the beam of length dx , as shown in Figure 3. The tension force, T , is assumed to be applied at the centroid of the cross-section and it acts in such a manner as to reduce the peak deflection of the beam. The deflection v is the displacement in the y -direction of any point on the axis of the beam. Here upwards forces and counterclockwise moments are taken as positive.

Equilibrium of forces in the vertical direction gives:

$$\sum F_{vert} = 0 \quad V - qdx - (V + dV) = 0$$

After simplification, this results in the following differential equation:

$$\frac{dV}{dx} = -q \quad (11)$$

Consider now the equilibrium of moments for the beam element about an axis at the left-hand side of the beam segment, where the axis is perpendicular to the plane of the figure. We obtain:

$$\sum M = 0 \quad -M - q dx \left(\frac{dx}{2}\right) - (V + dV)dx + (M + dM) - T dv = 0$$

Discarding second-order terms that involve products of differentials ($dx dx$ and $dV dx$) because they are negligible in size compared to the other terms, after simplification this results in the following differential equation:

$$\frac{dM}{dx} = V + T \frac{dv}{dx} \quad (12)$$

Assuming that the strains are small, and in keeping with the inherent assumptions of classical Euler-Bernoulli beam theory (i.e. plane sections remain plane and normal to the

deflected neutral axis) [1], the bending moment M is proportional to the curvature κ of the beam:

$$M = EI\kappa, \quad \kappa = \frac{\frac{d^2v}{dx^2}}{\left[1 + \left(\frac{dv}{dx}\right)^2\right]^{3/2}} \quad (13)$$

For a long and slender beam, the slope anywhere along the beam will be small, so that $\left(\frac{dv}{dx}\right)^2 \ll 1$, which leads to the following equation for the bending moment:

$$M = EI \frac{d^2v}{dx^2} \quad (14)$$

By taking a derivative operation of the left-hand and right-hand sides of Equation (12), and considering Equations (11) and (14), the differential form of the beam equilibrium equation can be written as:

$$\frac{d^2}{dx^2} \left(EI \frac{d^2v}{dx^2} \right) - T \frac{d^2v}{dx^2} = -q(x) \quad (15)$$

For the present beam problem, considering that EI and $q(x) = W$ remain constant for $0 \leq x \leq L$, Equation (15) can be rewritten as:

$$EI \frac{d^4v}{dx^4} - T \frac{d^2v}{dx^2} = -W \quad (16)$$

Considering that $T > 0$, and letting $k^2 = \frac{T}{EI}$, Equation (16) can be further rewritten as:

$$\frac{d^4v}{dx^4} - k^2 \frac{d^2v}{dx^2} = -\frac{W}{EI} \quad (17)$$

The general solution to the differential equation in Equation (17) is:

$$v(x) = ae^{kx} + be^{-kx} + cx + d + \frac{W}{2T}x^2 \quad (18)$$

The first and second derivatives of $v(x)$ are:

$$\frac{dv}{dx} = ake^{kx} - bke^{-kx} + c + \frac{W}{T}x \quad (19)$$

$$\frac{d^2v}{dx^2} = ak^2e^{kx} + bk^2e^{-kx} + \frac{W}{T} \quad (20)$$

Accordingly, the distribution of the shear force $V(x)$ is solved based on Equation (12) as follows:

$$V(x) = -Wx - cT \quad (21)$$

The boundary conditions corresponding to the deflections, slopes and curvatures of the beam can be deduced from Figure 2, and they are as follows:

$$\text{At } x = 0, v = 0 \text{ and } \frac{dv}{dx} = 0$$

$$\text{At } x = L, v = 0 \text{ and } \frac{d^2v}{dx^2} = 0$$

Using the above four boundary conditions, the four coefficients a , b , c , and d in the expression for the beam deflection can be solved analytically using Equation (22):

$$\begin{bmatrix} 1 & 1 & 0 & 1 \\ k & -k & 1 & 0 \\ e^{Lk} & e^{-Lk} & L & 1 \\ k^2 e^{Lk} & k^2 e^{-Lk} & 0 & 0 \end{bmatrix} \begin{bmatrix} a \\ b \\ c \\ d \end{bmatrix} = \begin{bmatrix} 0 \\ 0 \\ -\frac{W}{2T} L^2 \\ -\frac{W}{T} \end{bmatrix} \quad (22)$$

The analytical solution to the above system of simultaneous equations was obtained using SymPy, which is a Python-based library for symbolic mathematics. The SymPy commands that were used to obtain the solution are described in Appendix A, and the solution that was obtained is presented below:

$$\begin{bmatrix} a \\ b \\ c \\ d \end{bmatrix} = -\frac{W}{T} \begin{bmatrix} \frac{L^2 k^2 - 2Lk e^{Lk} + 2e^{Lk} - 2}{2k^2 (Lk e^{2Lk} + Lk - e^{2Lk} + 1)} \\ \frac{(L^2 k^2 e^{Lk} + 2Lk - 2e^{Lk} + 2)e^{Lk}}{2k^2 (Lk e^{2Lk} + Lk - e^{2Lk} + 1)} \\ \frac{L^2 k^2 e^{2Lk} + L^2 k^2 - 2e^{2Lk} + 4e^{Lk} - 2}{2k (Lk e^{2Lk} + Lk - e^{2Lk} + 1)} \\ \frac{-L^2 k^2 (e^{2Lk} - 1) - 4Lk e^{Lk} + 2e^{2Lk} - 2}{2k^2 (Lk e^{2Lk} + Lk - e^{2Lk} + 1)} \end{bmatrix} \quad (23)$$

The supporting force, R_p , at the propped end of the beam can be obtained by substituting $x = L$ into Equation (21), noting that the "+" direction of R_p is upwards, $R_p = -V|_{x=L}$.

In order to determine the maximum deflection of the beam, δ_{max} , the slope dv/dx in Equation (19) is set equal to zero:

$$ake^{kx} - bke^{-kx} + c + \frac{W}{T}x = 0 \quad (24)$$

and we then solve for the distance $x = x_{\delta_{max}}$ to the point of maximum deflection.

Equation (24) is highly nonlinear, so a simple closed-form analytical solution probably does not exist. However, it is possible to obtain a solution using numerical techniques. One such numerical method is the bisection method [3], which is also relatively easy to program. When using the bisection method to obtain a solution to Equation (24), convergence was rapid, with a solution that is accurate to 5 significant figures typically being obtained in a few tens of iterations.

Once the value of $x_{\delta_{max}}$ has been calculated, the maximum deflection is determined as:

$$\delta_{max} = -v(x_{\delta_{max}}) \quad (25)$$

The negative sign in the above equation takes into account that the deflection is downwards.

The tip deflection of an encastre cantilever beam under uniform transverse load W whose tip is free of restraint is given using the following formula [2]:

$$\delta_{tip} = \frac{WL^4}{8EI} \quad (26)$$

3.3 Nonlinear FEA solution for tension force $T \geq 0$ case

The Abaqus 6.14-2 finite element analysis code was used to solve the nonlinear beam problem depicted in Figure 2 for a range of values of the tension force, T . One end of the beam was modelled as being encastre, while the opposite end where the cable tension force is being applied was restrained using a roller-type constraint, which permitted axial movement but no vertical movement. The encastre end of the beam therefore has both horizontal and vertical reaction force components, as well as sustaining a bending moment. The roller-type constraint at the opposite end of the beam produces a vertical reaction force.

The beam of length $L = 4500$ mm was subdivided into 4500 elements of equal length, although many fewer elements could easily have been used to obtain an accurate enough solution. It was decided to use a 1-mm element length in order to avoid the task of having to interpolate the deflected shape in order to accurately determine the peak deflection and its location along the span of the beam.

The Abaqus beam element type B23 was used, which corresponds to a 2-noded beam element that uses cubic interpolation. The cross-sectional dimensions of the beam were input using the pipe profile option that automatically handles circular cross-sections. The formulation chosen to be used was the thick-walled option.

Two load steps were used during the analysis. The first consisted of 10 load increments that were used to ramp up the distributed load from a starting value of zero to its final value of W . Once the full amplitude of the distributed loading was reached, the second analysis step was used to apply the tension force using 50 load increments, covering the load range $0 \text{ N} \leq T \leq 25000 \text{ N}$ in steps of 500 N.

The total CPU time that was required in order to obtain a solution was about 70 seconds or so on a Hewlett-Packard Z800 Workstation that was fitted with Intel Xeon X5690 3.47 GHz processors. A converged solution at each load increment was obtained during the first iteration for all but two of the load increments.

3.4 Computed analytical and nonlinear FEA results

The collection of analytical equations for the Euler-Bernoulli beam solutions obtained for the cases $T = 0$ and $T > 0$ were programmed as VBA functions in a Microsoft Excel spreadsheet. A listing of the source code for the various functions is provided in Appendix B.

The analytical solutions were computed for a range of values of the tension force $T = 0$ N, 2500 N, 5000 N, 10000 N, 15000 N, 20000 N and 25000 N. The analytical results are compared to the values obtained from the Abaqus nonlinear finite element beam analysis in Table 1. The results presented here include δ_{max} , $x_{\delta_{max}}$, R_p , R_e , M_e , and θ_p . It is clear that there is excellent agreement between the two sets of results, with the maximum difference between the solutions being only a very small 0.052%.

For an axial tension force of $T = 0$ N, the maximum deflection is $\delta_{max} = 5.51$ mm, while for $T = 25000$ N it has reduced to $\delta_{max} = 1.64$ mm. This is a significant reduction of about 70%. In addition, it is to be noted that the rotation angle of the beam at the propped end is very small ($\theta_p = 0.27^\circ$ for $T = 0$ N), which is in keeping with the previously mentioned assumptions of Euler-Bernoulli beam theory for long and slender beams. For an equivalent encastre cantilever beam whose tip is free of restraint, for the case without any axial tension force the tip deflection is calculated using Equation (26) to be $\delta_{tip} = 127.2$ mm. As expected, this is much greater than the maximum deflection experienced by the propped cantilever beam.

Figure 4 shows the computed deflection shapes $v(x)$ of the propped cantilever beam for various values of applied tension force T that were obtained from the analytical and nonlinear FEA solutions. The agreement between the two sets of results is excellent.

The relationship between the maximum deflection δ_{max} and the applied tension force T is shown in Figure 5. It is seen that the maximum deflection decreases nonlinearly with increasing tension force, but the rate of decrease tapers off. The agreement between the analytical and the nonlinear FEA results is once again excellent.

The relationship between the supporting force R_p at the propped end of the cantilever beam and the applied tension force T is shown in Figure 6. It is seen that the supporting force increases slowly with increasing tension force. The agreement between the analytical and the nonlinear FEA results is excellent.

The relationship between the x -position $x_{\delta_{max}}$ of the maximum beam deflection δ_{max} and the applied tension force T is shown in Figure 7. It is seen that the location of the point of peak deflection moves slowly towards the encastre end of the beam with increasing tension force. The agreement between the analytical and the nonlinear FEA results is excellent.

Figure 8 shows the variation in the values of the reaction force R_e and reaction moment M_e at the encastre end of the beam as a function of the applied tension force T . The supporting force R_p is also shown for completeness and ease of comparison. Once again, the agreement between the analytical and the nonlinear FEA results is excellent.

Figure 9 shows the computed shear force diagrams $V(x)$ for various values of applied tension force T . It is evident that the levels of tension force that are considered here have a relatively small effect on the shear force distribution along the length of the beam. For the case $T = 0$, the shear force diagram presented here corresponds to the one published by Gere and Timoshenko [2] for their propped cantilever example in Figure 10-7. For the case

$T = 0$, the zero crossing is located at $x = 0.625L$, and it progressively moves towards the encastre end of the beam as the tension force is increased.

Figure 10 shows the computed bending moment diagrams $M(x)$ for various values of the applied tension force T . It is evident that the levels of tension force that are considered here have a significant effect on the bending moment distribution along the length of the beam. For the case $T = 0$, the bending moment diagram presented here corresponds to the one published by Gere and Timoshenko [2] in their propped cantilever example in Figure 10-7. For the case $T = 0$, the zero crossing in the bending moment occurs at $x = 0.250L$, while the point of inflection is at $x = 0.625L$. As the tension force increases, both the zero crossing and the point of inflection in the $M(x)$ curve move towards the encastre end of the beam.

4. Dynamic analysis

In the preceding section, the static deflection responses of the static pressure pipe were computed. For the purpose of that analysis, the pipe was idealised as a slender propped cantilever beam, fixed at one end and roller-supported at the other, with a horizontal tension force applied at the roller-supported end, as depicted in Figure 2. This configuration was considered to be a sufficiently accurate idealisation of the actual structural configuration shown in Figure 1, whereby the tension loads that exist in the multiple supporting cables have been resolved into a single horizontally-applied net tension force T .

It is considered here that the slender propped cantilever beam idealisation described in the previous paragraph is equally applicable to a dynamic analysis of the modal response of the static pressure pipe. It is recognised that the system of supporting tension cables has an attendant mass and compliance. However, the magnitude of any displacement of the propped end of the beam is expected to be altogether negligible in comparison with the amplitude of transverse vibration when the beam is vibrating at its first natural frequency. As a consequence, it may be expected that any dynamic coupling between the response of the beam and the cable support system will be small and will therefore have a second-order effect on the dynamic response of the beam, especially at the lowest natural frequency, which is the one of greatest interest.

4.1 Analytical modal solution for tension force $T = 0$ case (textbook)

It is possible for a beam to vibrate laterally at an infinite number of natural frequencies. At each natural frequency of vibration, the shape of the beam will take on a particular characteristic shape. Each of these shapes is called a normal mode of vibration, and is the deflected shape of the beam when it is vibrating harmonically.

Young and Felgar [4] have computed equations and tables of characteristic functions representing the undamped normal modes of transverse vibration of uniform beams for a range of different specified end conditions. One of the cases that they studied included that of a propped cantilever beam (which they termed a clamped-supported beam).

The undamped natural frequency f_n in hertz of the n^{th} mode of vibration of a propped cantilever beam in the absence of any axial tension force is given by the following equation:

$$f_n = \frac{1}{2\pi} \beta_n^2 \sqrt{\frac{EI}{m/L}} \quad (27)$$

where m is the mass of the beam. The characteristic shape of the n^{th} mode of vibration of a propped cantilever beam in the absence of any axial tension force is given by the following equation:

$$\psi_n = \cosh \beta_n x - \cos \beta_n x - \alpha_n (\sinh \beta_n x - \sin \beta_n x) \quad (28)$$

The values of $\beta_n L$ and α_n for the first 8 modes of vibration for a propped cantilever beam are presented in Table 2 [4, 5, 6], and the values of $\beta_n L$ correspond to solutions of a transcendental equation of the form $\tan(\lambda) = \tanh(\lambda)$ [6]. Young and Felgar [4] have provided the numerical values of $\beta_n L$ and α_n for the first 5 modes, and then offered the following equations for $n > 5$:

$$\beta_n L \cong \frac{\pi}{4} (4n + 1) \quad (29)$$

$$\alpha_n \cong 1 \quad (30)$$

Inspection of the values presented in Table 2 shows that Equations (29) and (30) are also quite accurate for $1 \leq n \leq 5$.

Blevins [6] has noted that, since the longitudinal displacement of straight beams during transverse vibration is of second order, the presence or absence of longitudinal displacement constraints does not affect the natural frequencies presented in Table 2.

4.2 Computed nonlinear FEA results for tension force $T \geq 0$ case (this study)

For the case of zero axial load ($T = 0$), Table 3 presents a comparison of the undamped natural frequencies f_n (in hertz) of the first eight transverse vibration modes of the static pressure pipe, modelled as a propped cantilever beam, computed analytically and using finite element beam analysis. It is evident that there is excellent agreement between the two sets of results. The analytically-computed lowest natural frequency is $f_1 = 7.618$ Hz, which is within 0.33% of the frequency that was computed using nonlinear FEA.

For a cantilever beam with a free end, the value of $\beta_n L$ for the first natural mode of vibration is $\beta_1 L = 1.8751$ [4]. For the present static pressure pipe, if the support at the propped end is removed, the first undamped natural frequency is calculated to be $f_1 = 1.737$ Hz. This is only 22.8% of the first natural frequency for the pipe when its end is propped, so it is evident that the addition of the propping support greatly increases the first natural frequency of the beam.

The natural frequencies f_n of the transverse natural vibration modes of the static pressure pipe were also computed using nonlinear finite element beam analysis for various values of axial tension force T . Figure 11 shows the variation of the frequency of the first natural vibration mode f_1 as a function of the applied tension force T , where $f_1 = 7.593$ Hz for $T = 0$ N and $f_1 = 13.878$ Hz for $T = 25000$ N.

A comparison of the natural frequencies for the first eight natural modes is shown in Table 4. Each natural frequency that was computed for a non-zero value of T , denoted here as $f_n|_{T=\dots}$, was normalised by the corresponding natural frequency of that mode obtained for zero axial tension force, $f_n|_{T=0}$. As expected, the results show that the natural frequencies of the static pressure pipe increase with increasing axial tension force. For a given axial tension force, it is noted that the percentage increase in frequency of each of the natural frequencies progressively reduces with the increasing order of the natural mode. For example, the first natural frequency is increased by 82.7% when $T = 25000$ N, while the frequency of the second natural mode has only increased by 36.2%.

The nondimensional characteristic mode shapes of the first three natural modes of the propped cantilever beam for axial tension loadings of $T = 0$ N and $T = 25000$ N are shown in Figure 12. The mode shape for the first natural mode is shown in the top picture, that for the second mode is shown in the middle picture, and that for the third mode is shown in the bottom picture. The first natural mode has one peak between the supports (which are located at $x = 0$ mm and $x = 4500$ mm), the second natural mode has two peaks, and so on. It is apparent that the effect of the axial tension force on the shape of the first mode is noticeable but relatively small, and the effect of axial tension on the mode shape becomes progressively less the higher the order of the mode.

For comparison purposes, the top picture in Figure 12 also includes the normalised static deflection shape of the propped cantilever beam under the action of the uniform distributed loading W for the $T = 0$ N case (the green dotted line). It is apparent that the static deflection shape, which can be computed using Equation (3), is in fact very similar to the characteristic shape of the transverse flexural vibration mode corresponding to the first natural frequency of vibration.

4.3 Empirical formula for calculation of beam natural frequency for tension force $T \geq 0$ case (this study)

When an axial tensile force T acts on a beam, the natural frequencies of the beam will be higher than those for the same beam in the absence of such a load. Harris and Piersol [5] have noted that, for a simple cantilever beam with a constant axial force T applied at the free end, the fundamental natural frequency has been derived by Timoshenko [7] to be:

$$f_1|_T = f_1|_{T=0} \sqrt{1 + \frac{5}{14} (TL^2/EI)} \quad (31)$$

where $f_1|_{T=0}$ is the frequency of the fundamental natural mode obtained for the case of zero tension force ($T = 0$).

Taking the above approach, it has been found here that the following empirical equation can be used to compute the natural frequency $f_n|_T$ of the n^{th} mode of vibration of the propped cantilever beam as a function of the tension force T :

$$f_n|_T = f_n|_{T=0} \sqrt{1 + \xi_n TL^2/EI} \quad (32)$$

where $f_n|_{T=0}$ is the frequency of the n^{th} natural mode obtained for the case of zero tension force ($T = 0$), which can be obtained from an FEA or by using Equation (27).

The values of $\xi_n n^2$ for the first eight natural modes are presented in Table 5. Here the values of ξ_n have been multiplied by n^2 as the resulting values of $\xi_n n^2$ are of a similar order of magnitude, and the asymptotic behaviour of $\xi_n n^2$ for higher values of n becomes apparent.

The values of $\xi_n n^2$ shown in Table 5 were determined by using the the Equation (32) and substituting the appropriate natural frequency values obtained from the nonlinear FEA for levels of tension force of $T = 0$ N and $T = 25000$ N:

$$n^2 \xi_n = n^2 \left[\left(\frac{f_n|_{T=25000}}{f_n|_{T=0}} \right)^2 - 1 \right] \frac{EI}{25000L^2} \quad (33)$$

For the first natural mode, the accuracy of Equation (32) is better than 0.48% with respect to the results from the nonlinear FEA. The accuracy is seen to improve further as the order of the mode under consideration is increased. As they are based on the results from the nonlinear FEA, the values of $\xi_n n^2$ are known to be valid for values of tension force in the range $0 \text{ N} \leq T \leq 25000 \text{ N}$.

The results produced by Equation (32) for the first three natural modes have been plotted in Figure 13 (red dotted lines), where it can be seen that there is excellent agreement with the results from the nonlinear FEA (solid black lines).

4.4 Calculation of cable natural frequency for $T \geq 0$ case (textbook)

It is also instructive to determine estimates of the natural frequencies of the four symmetrically-arranged steel tension cable restraints. These cables are approximately 2.5 mm in diameter and they each have a length of $L_c = 2.3$ metres. The estimated mass per unit length of the cables is approximately $\mu_c = 0.0384$ kg/m.

For the geometric layout depicted in the side view shown in Figure 1, the tension T_c in each of the four cables is given by the following equation:

$$T_c = \frac{\sqrt{3}}{4} T \quad (34)$$

For a simply-supported flexible cable of length L_c being stretched under the action of a tension force T_c , Blevins [6] gives the following equation for the n^{th} natural frequency of the cable:

$$f_{cn} = \frac{n}{2L_c} \sqrt{\frac{2T_c}{\mu_c}} \quad n = 1, 2, 3, \dots \quad (35)$$

where μ_c is the mass per unit length of the cable.

Figure 14 shows the variation in the natural frequency of the cables for the first three natural modes. For a moderate value of axial tension load of $T = 5000$ N, the first natural frequency of the cable is $f_{c1} = 73.0$ Hz. This frequency is 7.94 times greater than the first natural frequency of the propped cantilever beam. When the axial tension force is increased to $T = 25000$ N, the first natural frequency of the cable increases to $f_{c1} = 163.2$ Hz. This frequency is 11.76 times greater than the first natural frequency of the propped cantilever beam. It is evident that, for potential working values of cable tension in the range $5000 \text{ N} \leq T \leq 25000 \text{ N}$, the first natural frequency of the cable will be well separated from the first natural frequency of the propped cantilever beam.

5. Conclusions

The general analytical solution for the deflection and supporting force of a slender propped cantilever beam has been derived using Euler-Bernoulli beam theory for a combined system of lateral and tensile axial loads. The validity of the analytical solution (static) was independently confirmed by cross-checking the results against those obtained from a nonlinear finite element analysis. The analytical solution (static) has been implemented in a Microsoft Excel spreadsheet, and it can easily be utilised for other beam geometries (e.g. a beam of a different length).

The computed results for the static pressure pipe from the static analysis show that:

1. As T increases from 0 N to 25000 N, the maximum deflection of the beam reduces from 5.52 mm to 1.64 mm.
2. The effect of T on reducing the maximum deflection is nonlinear, and the law of "diminishing returns" begins to apply at higher levels of T .
3. As T increases from 0 N to 25000 N, the reaction force R_p at the propped end of the beam increases from 43.0 N to 50.5 N. This indicates that R_p has a weak dependence on the tension force.

The results from the dynamic analysis of the static pressure pipe show that:

1. The frequency of the first natural mode of the beam is 7.6 Hz for the case of zero axial tension force. This increases to 13.9 Hz when the axial tension force is $T = 25000$ N, an increase of almost 83%. The frequencies of the higher-order natural modes of the beam are progressively less affected by the application of the axial tension force.
2. An empirical formula has been developed for the calculation of the natural frequencies $f_n|_T$ of the beam for $T \geq 0$.

3. The frequency of the first natural mode of the cable is $f_{c1} = 73.0$ Hz for $T = 5000$ N, and increases to $f_{c1} = 163.2$ Hz when $T = 25000$ N.
4. The frequency of the first natural mode of the cable is 7.94 times greater than the first natural frequency of the propped cantilever beam when $T = 5000$ N.

6. References

1. Bauchau, O. A., Craig, J. I. (2009). Euler-Bernoulli beam theory. In O. A. Bauchau and J. I. Craig (Eds.), *Structural Analysis: With Applications to Aerospace Structures* (pp. 173–221). Dordrecht, Springer, Netherlands. ISBN: 9789048125166. DOI: 10.1007/978-90-481-2516-6_5.
2. Gere, J. M., Timoshenko, S. P. (1997). *Mechanics of Materials*. 4th Edition, PWS Publishing, Boston, MA, USA. ISBN: 0-534-93429-3.
3. Teodorescu, P., Stănescu, N.-D., Pandrea, N. (2013). *Numerical Analysis: With Applications in Mechanics and Engineering*. IEEE Press, John Wiley & Sons Inc., New Jersey, USA. ISBN: 9781118077504.
4. Young, D., Felgar, Jr., R. P. (1949). *Tables of characteristic functions representing normal modes of vibration of a beam*. The University of Texas Publication, No. 4913.
5. Harris, C. M. (Ed.), Piersol, A. G. (Ed.) (2002). *Harris' Shock and Vibration Handbook*. Fifth Edition, McGraw-Hill, New York, USA. ISBN: 0-07-137081-1.
6. Blevins, R. D. (1979). *Formulas for natural frequency and mode shape*. Robert E. Krieger Publishing Company, Malabar, Florida, USA. ISBN: 0-89874-791-0.
7. Timoshenko, S. (1955). *Vibration Problems in Engineering*. 3rd Edition, Van Nostrand Company, Inc., Princeton, New Jersey, USA.

Table 1: Maximum beam deflection and its location, reaction forces and moments, and angle of rotation of the propped end of the beam, as obtained from the analytical and finite element solutions for various tension loads T .

T (N)	Result Type	δ_{max} (mm)	$x_{\delta_{max}}$ (mm)	R_p (N)	R_e (N)	M_e (N mm)	θ_p (degrees)
0	Analytical	5.51110	2603.1	42.9773	71.6288	64466	0.26991
	FEA	5.51108	2603.0	42.9778	71.6287	64466	0.26991
2500	Analytical	4.44231	2586.1	44.8975	69.7085	55825	0.21653
	FEA	4.44166	2586.0	44.9031	69.7073	55821	0.21650
5000	Analytical	3.72340	2571.1	46.2285	68.3775	49835	0.18081
	FEA	3.72354	2571.0	46.2281	68.3778	49841	0.18082
10000	Analytical	2.81683	2545.9	47.9794	66.6266	41956	0.13610
	FEA	2.81701	2546.0	47.9790	66.6270	41964	0.13611
15000	Analytical	2.26805	2525.4	49.1014	65.5046	36907	0.10926
	FEA	2.26834	2525.0	49.1009	65.5053	36919	0.10927
20000	Analytical	1.89982	2508.4	49.8951	64.7109	33335	0.09137
	FEA	1.90018	2508.5	49.8945	64.7117	33349	0.09138
25000	Analytical	1.63544	2493.9	50.4937	64.1123	30642	0.07859
	FEA	1.63586	2494.0	50.4926	64.1133	30658	0.07861

Table 2: Values of $\beta_n L$ and α_n for the first eight natural modes of a propped cantilever beam [4].

n	$\beta_n L$	α_n
1	3.9266	1.00078
2	7.0686	1.00000
3	10.2102	1.00000
4	13.3518	1.00000
5	16.4934	1.00000
6	19.6350	1.00000
7	22.7765	1.00000
8	25.9181	1.00000

Table 3: Comparison of the natural frequencies of the transverse vibration modes of the static pressure pipe computed analytically and using finite element beam analysis, for the case of zero axial force.

n	f_n Analytical (Hz)	f_n FEA (Hz)	Difference
1	7.618	7.593	-0.33%
2	24.69	24.63	-0.24%
3	51.51	51.45	-0.12%
4	88.08	88.02	-0.07%
5	134.4	134.4	-0.04%
6	190.5	190.4	-0.03%
7	256.3	256.3	0.00%
8	331.9	331.9	0.00%

Table 4: Comparison of the natural frequencies f_n of the transverse natural vibration modes of the static pressure pipe computed using finite element beam analysis for various values of axial tension force T (N).

n	$f_n _{T=0}$ (Hz)	$\frac{f_n _{T=2500}}{f_n _{T=0}}$	$\frac{f_n _{T=5000}}{f_n _{T=0}}$	$\frac{f_n _{T=10000}}{f_n _{T=0}}$	$\frac{f_n _{T=15000}}{f_n _{T=0}}$	$\frac{f_n _{T=20000}}{f_n _{T=0}}$	$\frac{f_n _{T=25000}}{f_n _{T=0}}$
1	7.593	1.116	1.217	1.397	1.555	1.698	1.828
2	24.63	1.043	1.083	1.159	1.230	1.297	1.361
3	51.45	1.022	1.043	1.083	1.122	1.159	1.196
4	88.02	1.013	1.026	1.050	1.075	1.098	1.121
5	134.4	1.009	1.017	1.034	1.050	1.066	1.082
6	190.4	1.006	1.012	1.024	1.036	1.048	1.059
7	256.3	1.005	1.009	1.018	1.027	1.036	1.045
8	331.9	1.004	1.007	1.014	1.021	1.028	1.035

Table 5: Values of $\xi_n n^2$ for the first eight natural modes of a propped cantilever beam with an axial tension force.

n	$\xi_n n^2$	Maximum error of Equation (32)
1	0.04746	0.48%
2	0.06910	0.11%
3	0.07834	0.05%
4	0.08348	0.03%
5	0.08680	0.02%
6	0.08911	0.01%
7	0.09084	0.01%
8	0.09205	0.01%

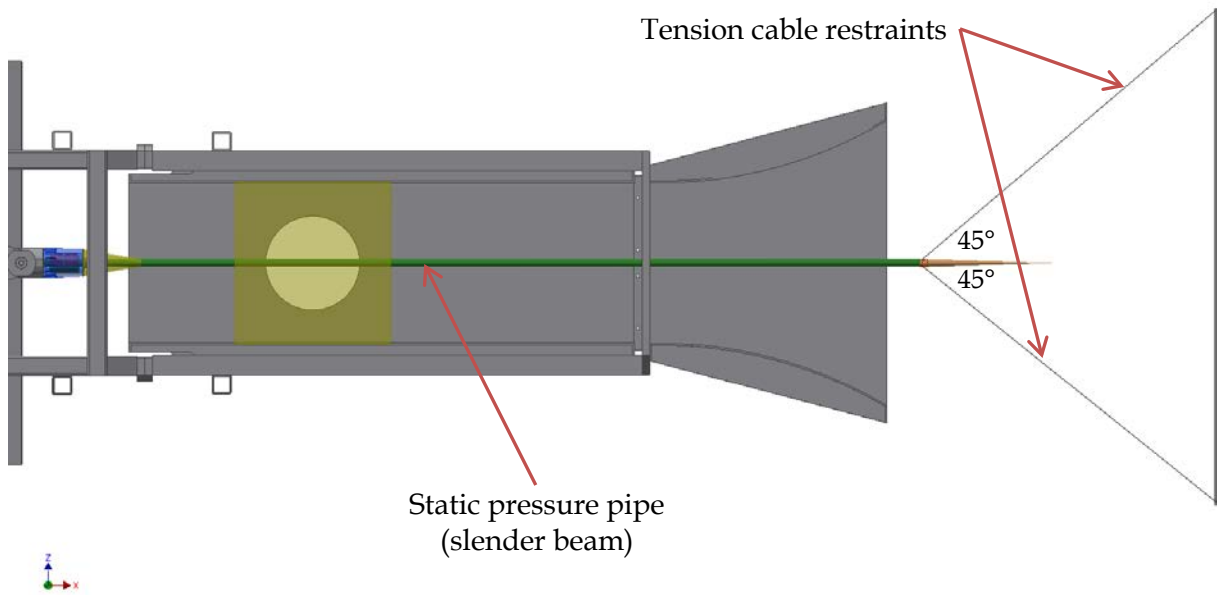


Figure 1: Layout diagram of the static pressure pipe installed in the DST Group Transonic Wind Tunnel aerodynamic testing facility.

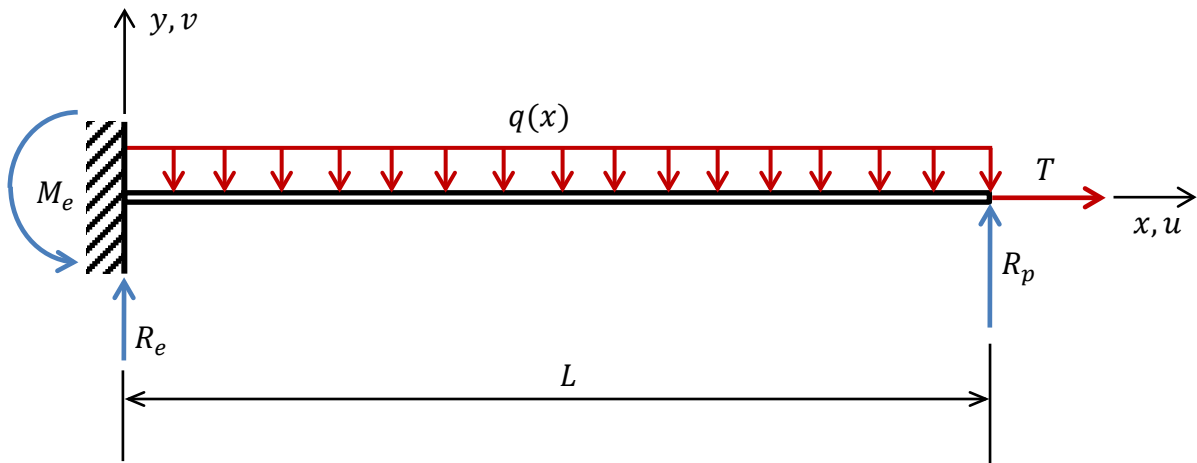


Figure 2: A slender beam under combined uniform transverse load $q(x)$ and tensile axial force T .

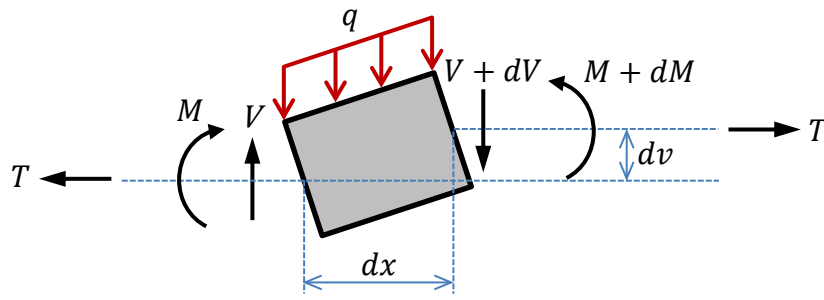


Figure 3: A beam segment of infinitesimally small length dx .

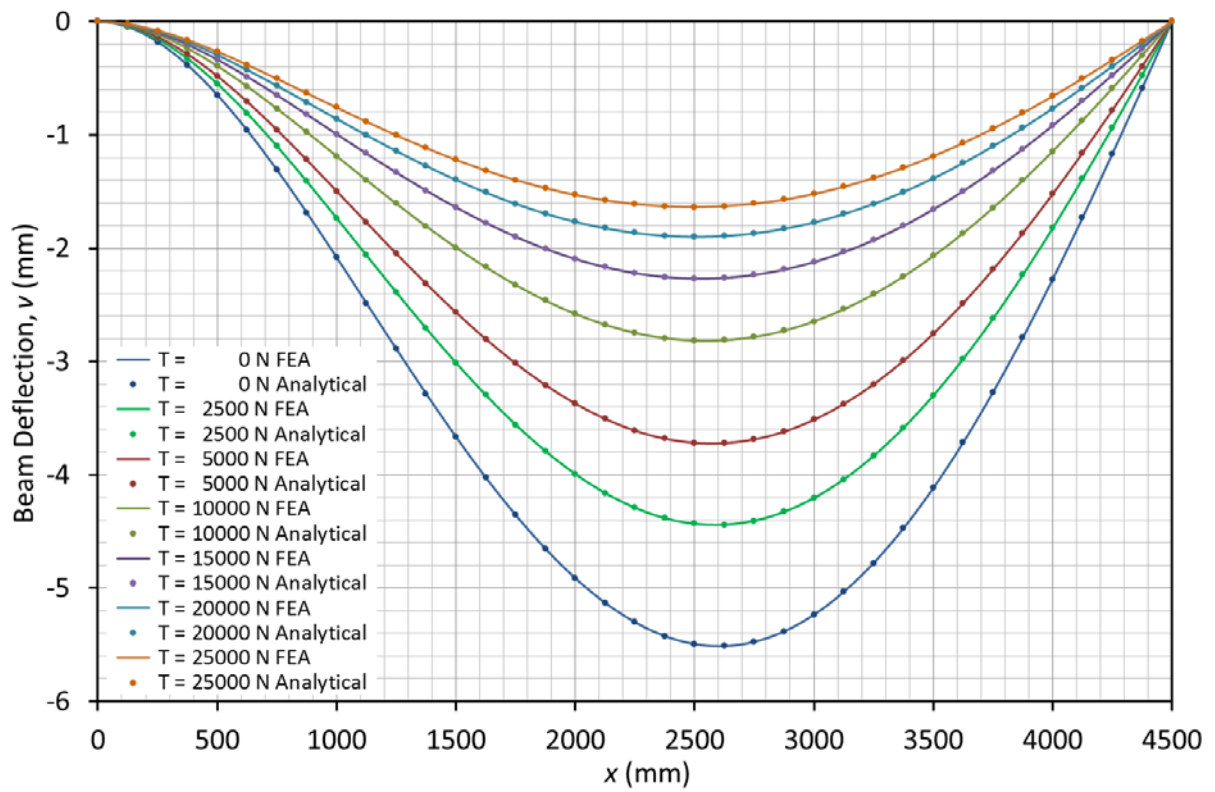


Figure 4: Beam deflection shape v for various values of applied tension force T .

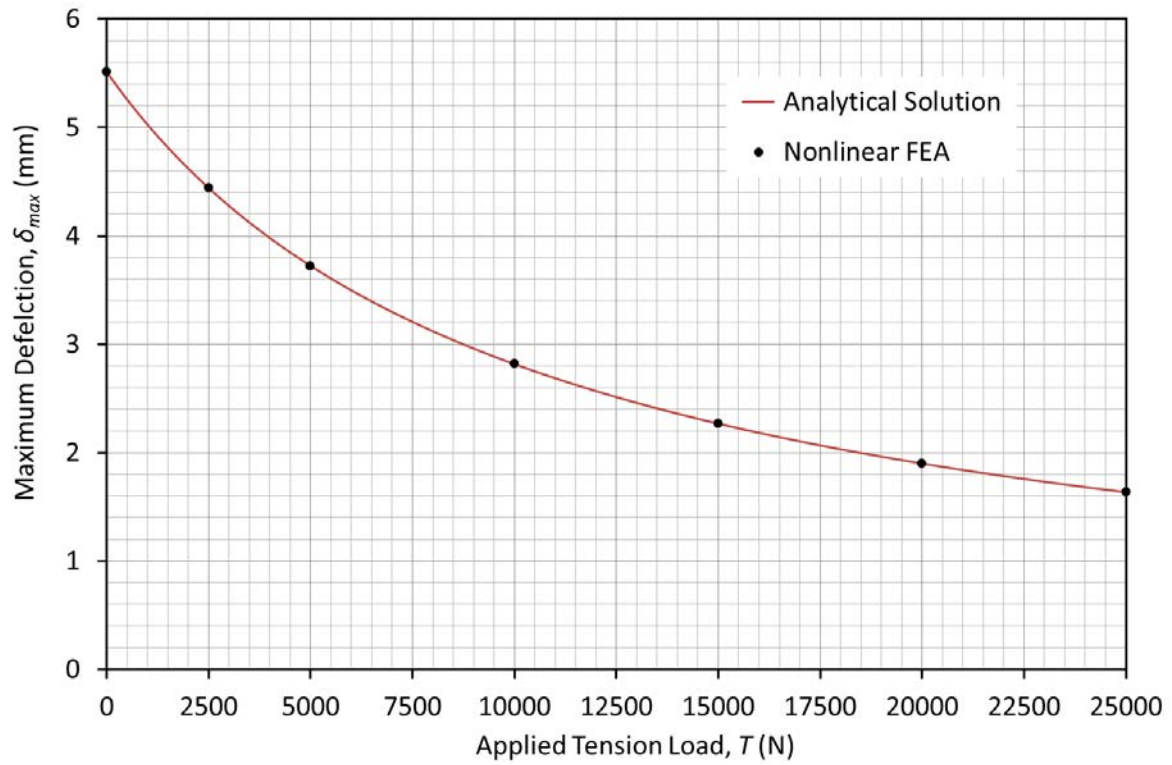


Figure 5: Relationship between maximum deflection δ_{max} and applied tension force T .

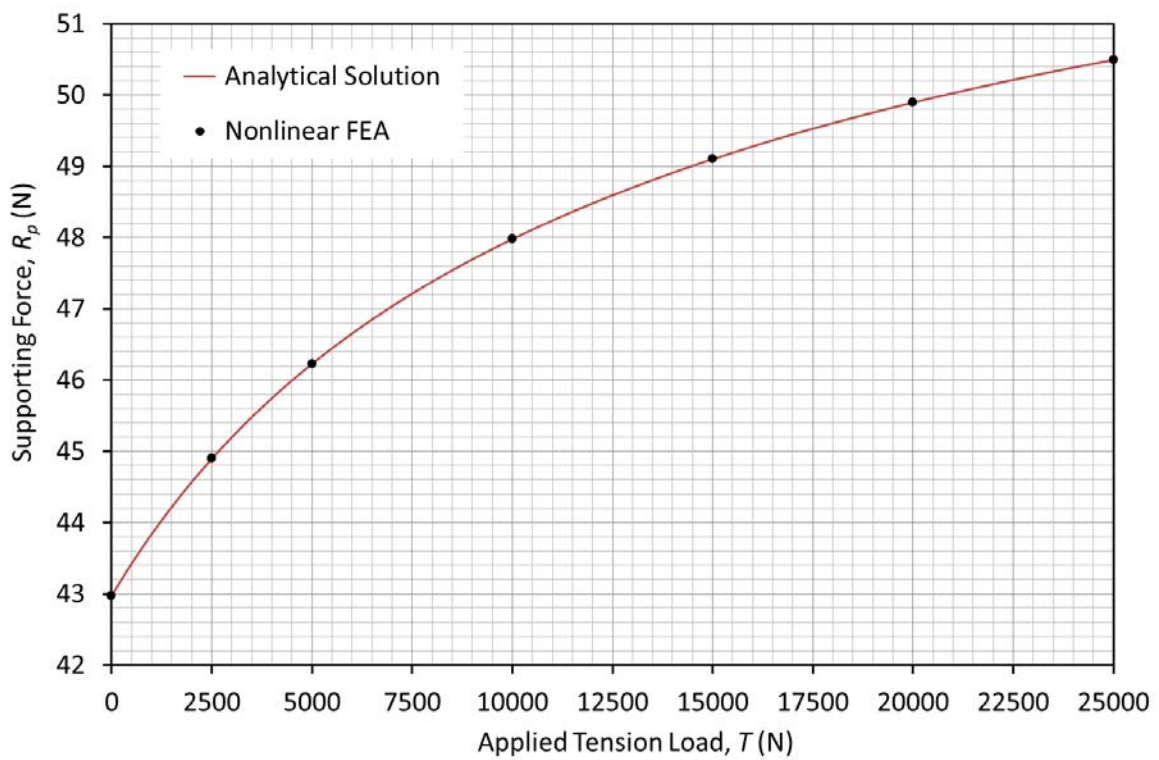


Figure 6: Relationship between supporting force R_p and applied tension force T .

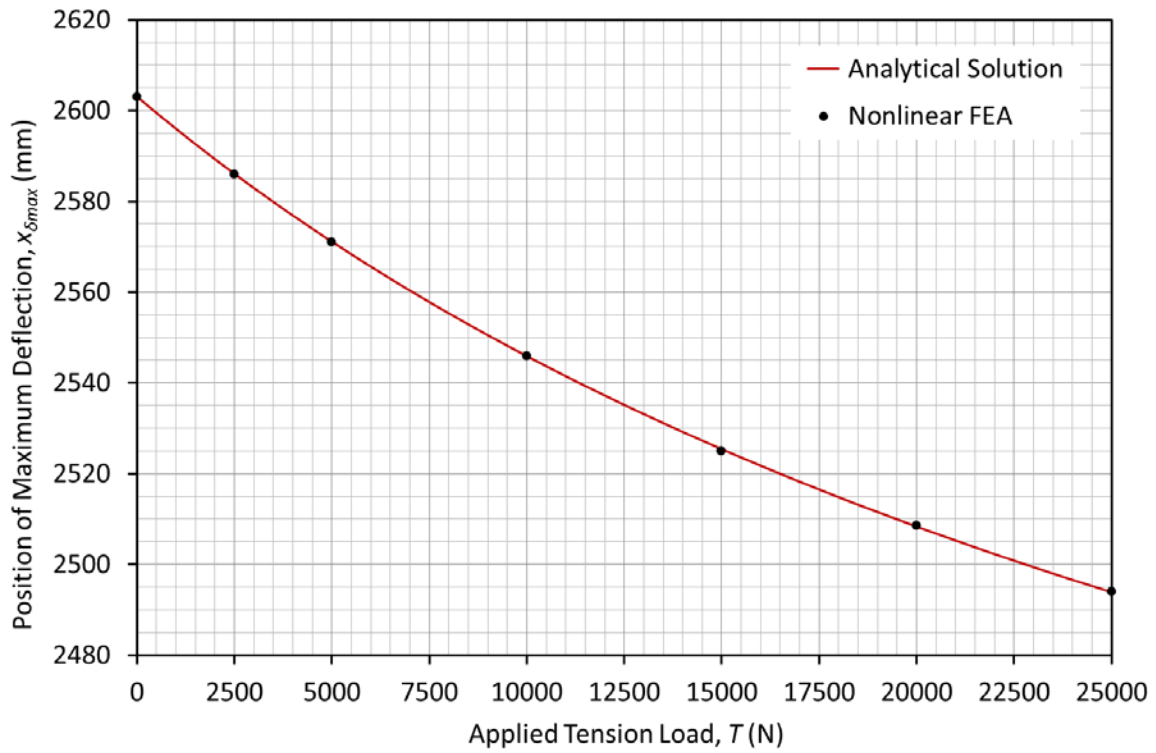


Figure 7: Variation in position of maximum deflection $x_{\delta_{max}}$ with applied tension force T .

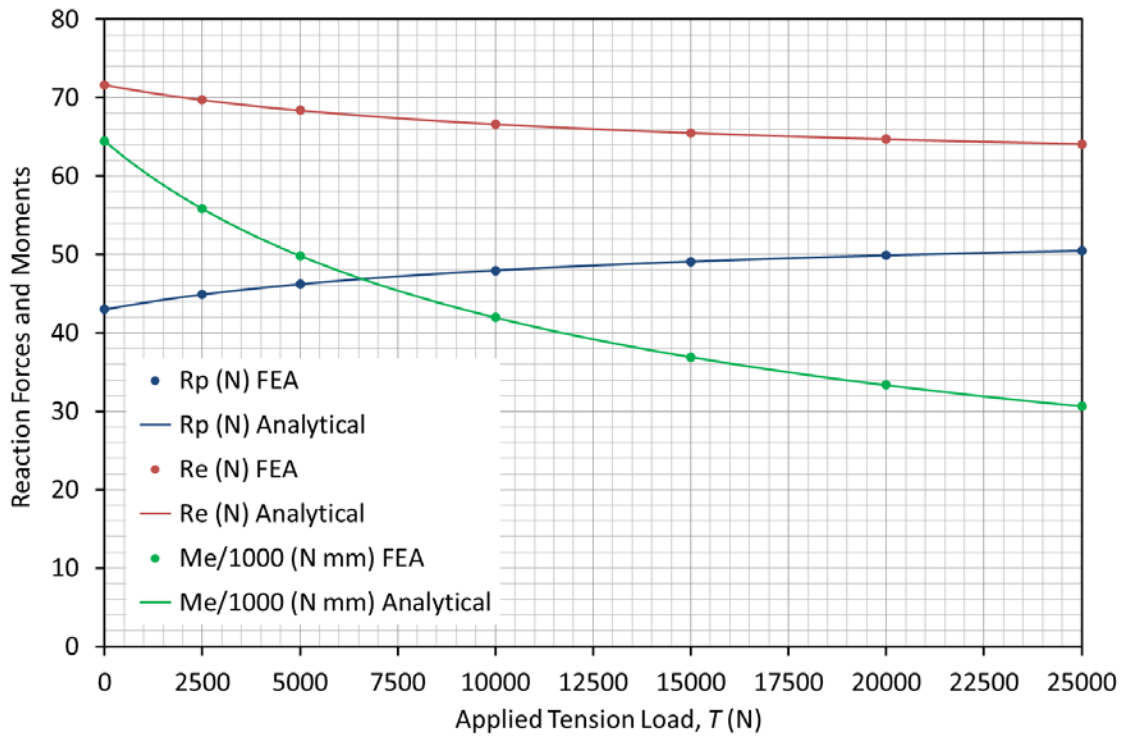


Figure 8: Variation of the reaction forces R_p and R_e and the reaction moment M_e as a function of applied tension force T .

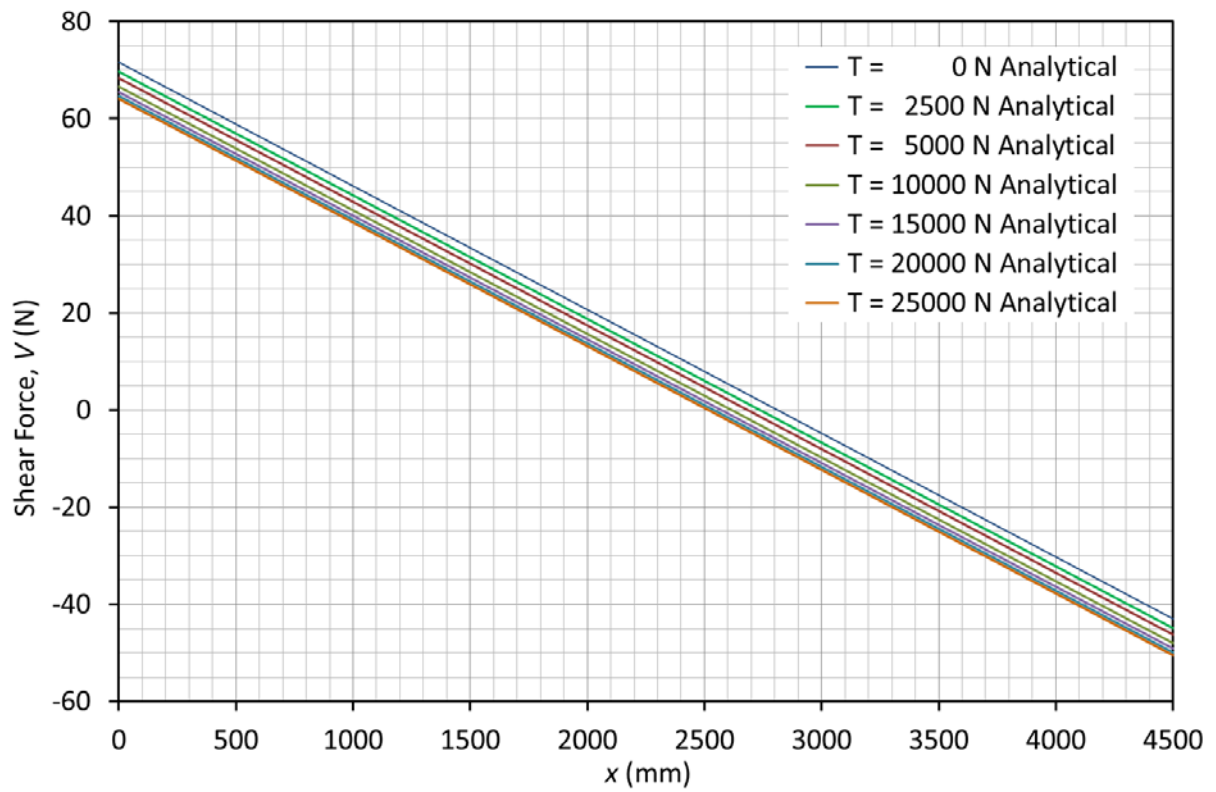


Figure 9: Shear force V diagrams for various values of applied tension force T .

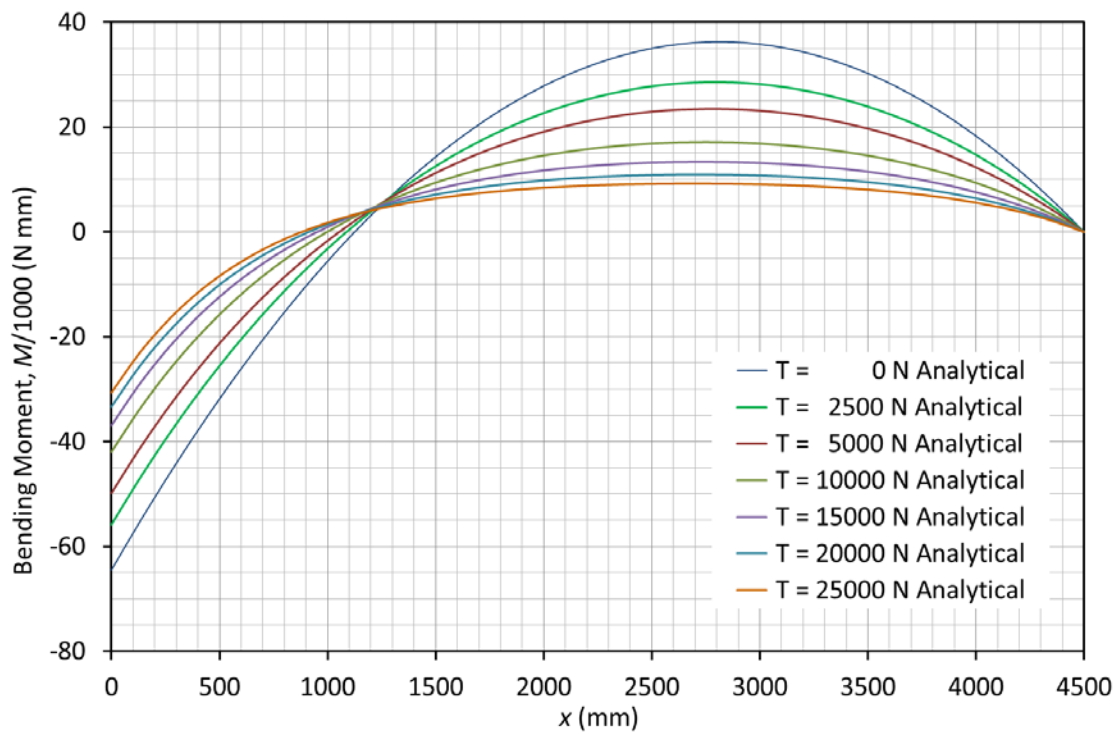


Figure 10: Bending moment M diagrams for various values of applied tension force T .

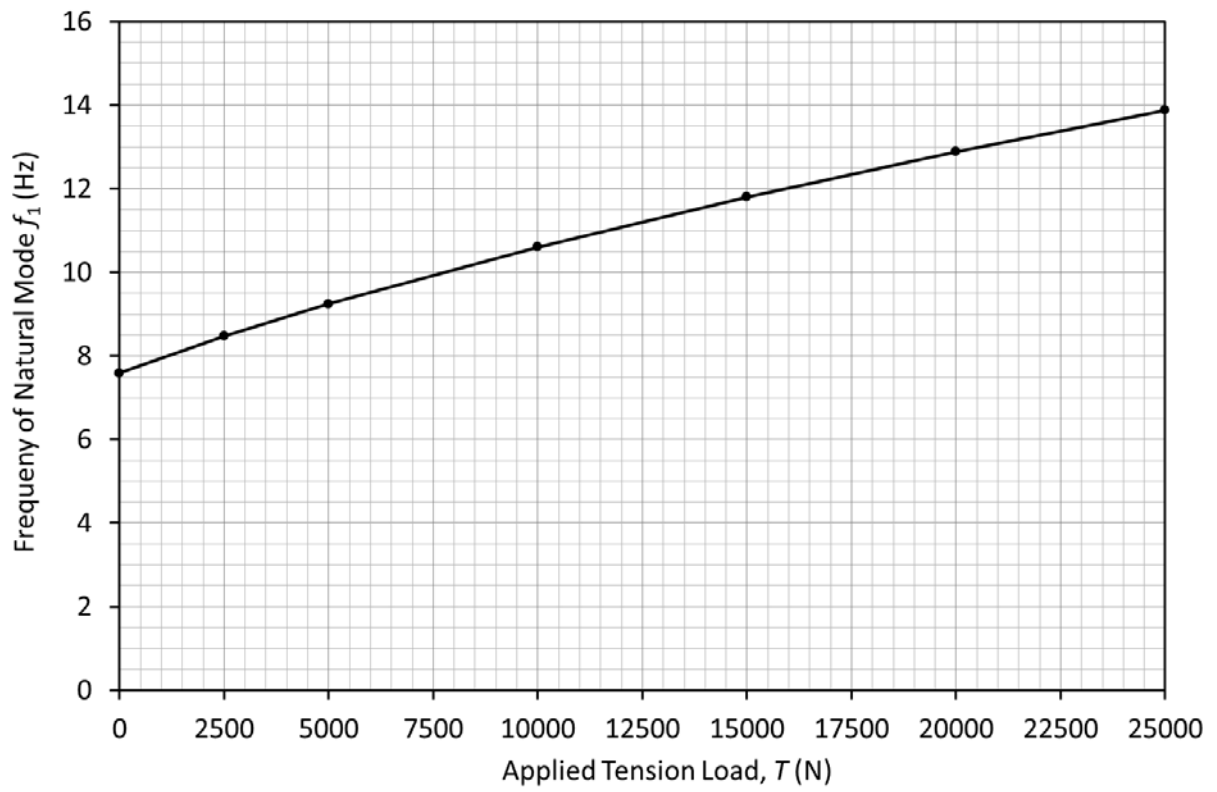


Figure 11: Variation of the frequency of the first natural vibration mode f_1 as a function of applied tension force T .

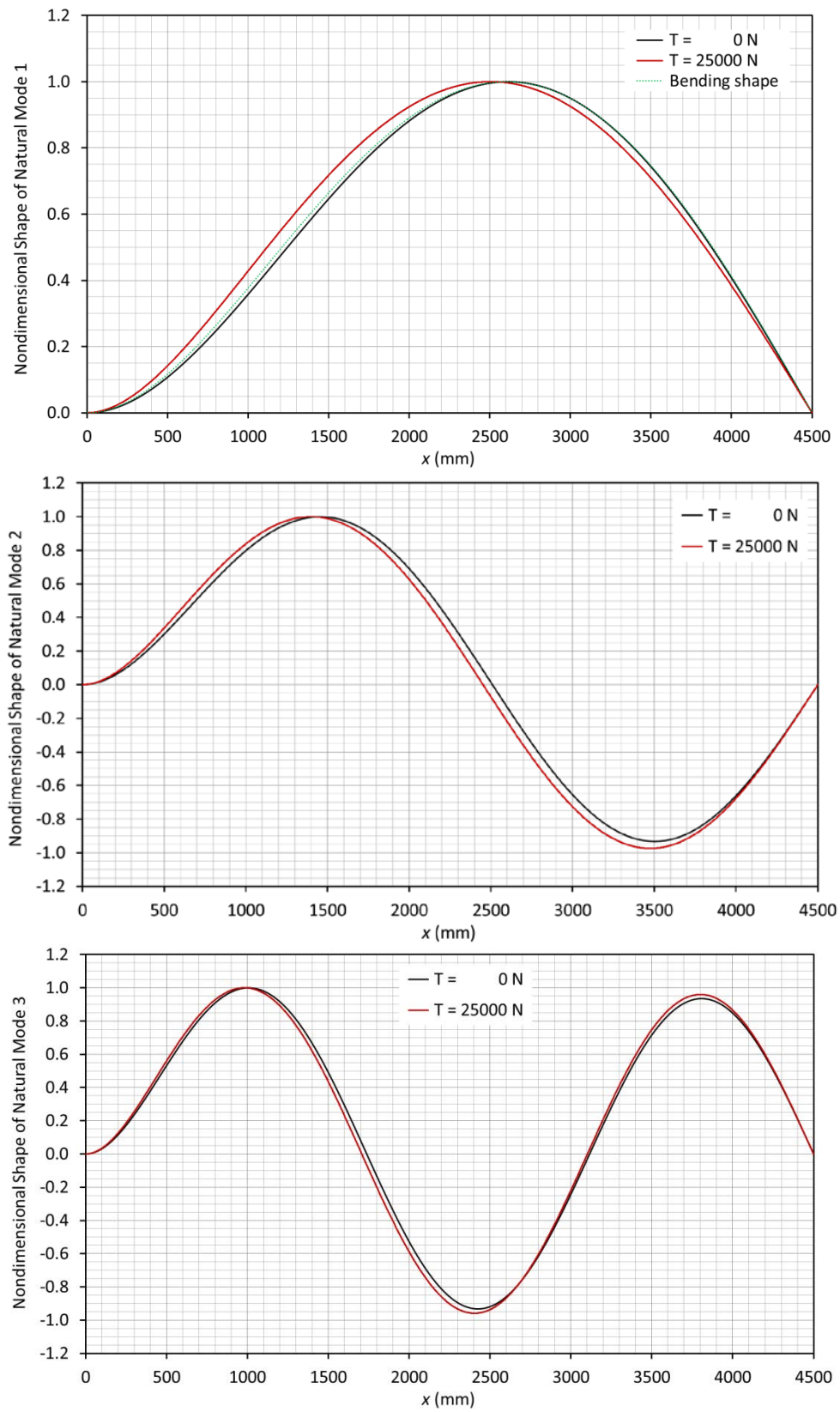


Figure 12: Nondimensional mode shapes of the first three natural modes of the propped cantilever beam for axial tension loadings of $T = 0$ N and $T = 25000$ N.

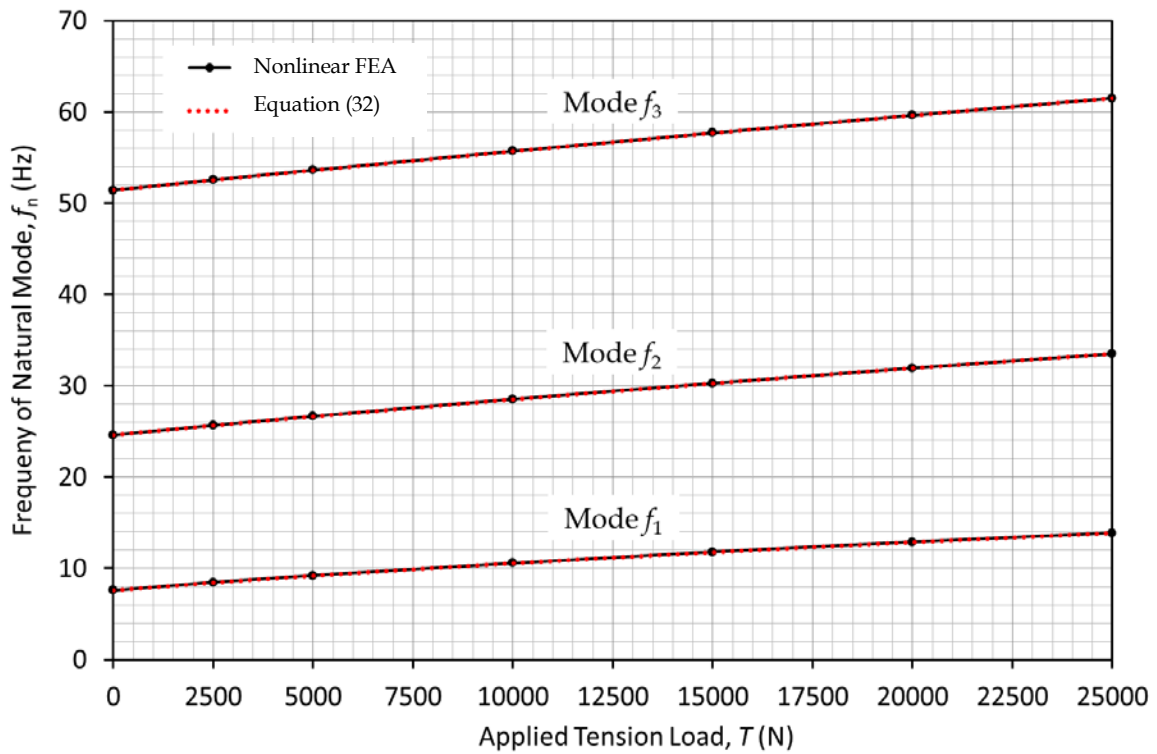


Figure 13: Variation in natural frequency obtained from the nonlinear FEA results compared to the predictions obtained using Equation (32) for the first three modes of the propped cantilever beam.

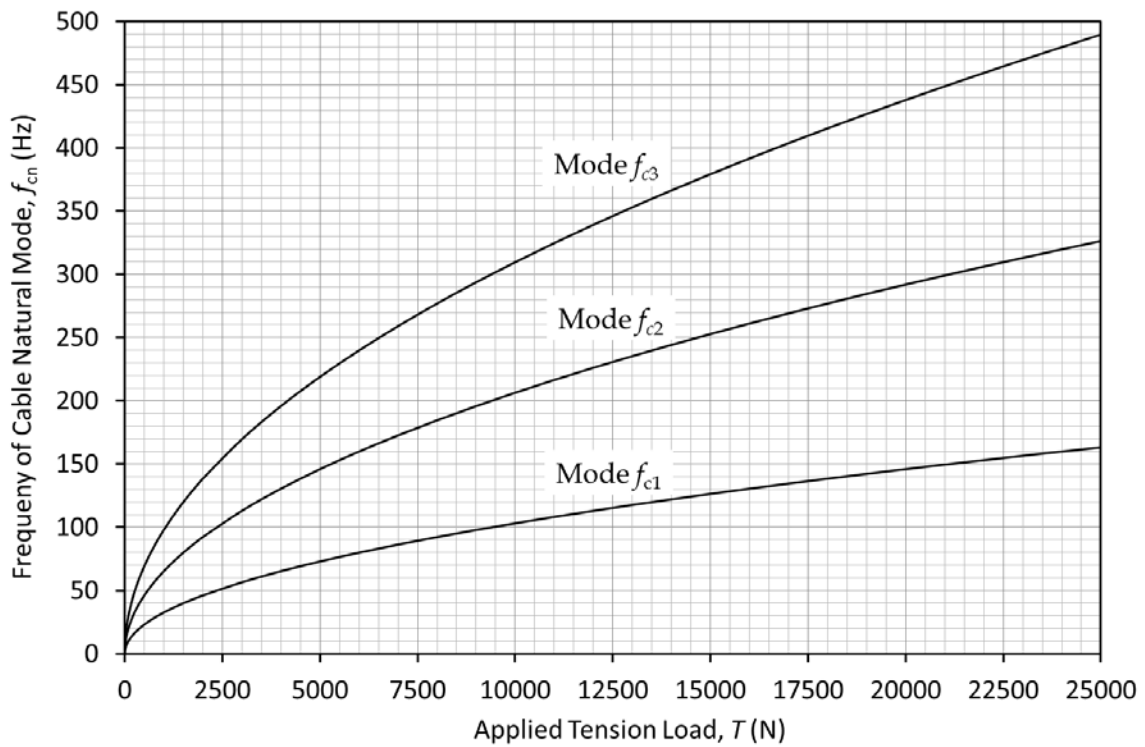


Figure 14: Variation in natural frequency of the first three natural modes of the cables as a function of the applied axial tension load in the beam.

Appendix A: Listing of SymPy symbolic computations

The SymPy package, which can be found at <http://www.sympy.org>, was used to perform the symbolic mathematical computations used to solve the system of simultaneous equations represented by Equation (22). The listing of the commands entered into SymPy (indicated by >>>) and the resulting output relating to the coefficients a , b , c , and d is presented below:

```
>>> from __future__ import division
>>> from sympy import *
>>>
>>> a,b,c,d = symbols('a b c d')
>>> L,k,W,T = symbols('L k W T')
>>> M = MatrixSymbol('M',4,4)
>>> RHS = MatrixSymbol('RHS',4,1)
>>> LHS = MatrixSymbol('LHS',4,1)
>>> M = Matrix([[1,1,0,1],[k,-k,1,0],[exp(L*k),exp(-
L*k),L,1],[k**2*exp(L*k),k**2*exp(-L*k),0,0]])
>>> RHS = Matrix([[0],[0],[-W*L**2/(2*T)],[-W/T]])
>>> LHS = M**-1*RHS
>>> LHS = simplify(LHS)
>>> a = LHS[0]
>>> b = LHS[1]
>>> c = LHS[2]
>>> d = LHS[3]
>>> a
W*(L**2*k**2 - 2*L*k*exp(L*k) + 2*exp(L*k) - 2)/(2*T*k**2*(L*k*exp(2*L*k) + L*k
- exp(2*L*k) + 1))
>>> b
-W*(L**2*k**2*exp(L*k) + 2*L*k - 2*exp(L*k) +
2)*exp(L*k)/(2*T*k**2*(L*k*exp(2*L*k) + L*k - exp(2*L*k) + 1))
>>> c
-W*(L**2*k**2*exp(2*L*k) + L**2*k**2 - 2*exp(2*L*k) + 4*exp(L*k) -
2)/(2*T*k*(L*k*exp(2*L*k) + L*k - exp(2*L*k) + 1))
>>> d
W*(L**2*k**2*(exp(2*L*k) - 1) + 4*L*k*exp(L*k) - 2*exp(2*L*k) +
2)/(2*T*k**2*(L*k*exp(2*L*k) + L*k - exp(2*L*k) + 1))
>>>
```

There is also a *SymPy Live* web page, which is located at <http://live.sympy.org/>, where a user can use an online version of SymPy. When the above SymPy commands were input, the same results as shown above were obtained, albeit with the expressions for the coefficients a , b , c , and d presented in mathematically-typeset text. The output screen from *SymPy Live* is shown below:

SymPy Live

Python console for SymPy 0.7.6 (Python 2.7.5)

These commands were executed:

```
>>> from __future__ import division
>>> from sympy import *
>>> x, y, z, t = symbols('x y z t')
>>> k, m, n = symbols('k m n', integer=True)
>>> f, g, h = symbols('f g h', cls=Function)
```

Documentation can be found at <http://docs.sympy.org/0.7.6>.

```
>>> a,b,c,d = symbols('a b c d')
>>> L,k,W,T = symbols('L k W T')
>>> M = MatrixSymbol('M', 4, 4)
>>> RHS = MatrixSymbol('RHS', 4, 1)
>>> LHS = MatrixSymbol('LHS', 4, 1)
>>> M = Matrix([[1, 1, 0, 1], [k, -k, 1, 0], [exp(L*k), exp(-L*k), L, 1], [k**2*exp(L*k), k**2*exp(-L*k), 0, 0]])
>>> RHS = Matrix([[0], [0], [-W*L**2/(2*T)], [-W/T]])
>>> LHS = M**-1*RHS
>>> LHS = simplify(LHS)
>>> a = LHS[0]
>>> b = LHS[1]
>>> c = LHS[2]
>>> d = LHS[3]
>>> a
```

$$\frac{W(L^2k^2 - 2Lke^{Lk} + 2e^{Lk} - 2)}{2Tk^2(Lke^{2Lk} + Lk - e^{2Lk} + 1)}$$

```
>>> b
```

$$\frac{W(L^2k^2e^{Lk} + 2Lk - 2e^{Lk} + 2)e^{Lk}}{2Tk^2(Lke^{2Lk} + Lk - e^{2Lk} + 1)}$$

```
>>> c
```

$$\frac{W(L^2k^2e^{2Lk} + L^2k^2 - 2e^{2Lk} + 4e^{Lk} - 2)}{2Tk(Lke^{2Lk} + Lk - e^{2Lk} + 1)}$$

```
>>> d
```

$$\frac{W(L^2k^2(e^{2Lk} - 1) + 4Lke^{Lk} - 2e^{2Lk} + 2)}{2Tk^2(Lke^{2Lk} + Lk - e^{2Lk} + 1)}$$

```
>>> |
```

Evaluate

Clear

Exit Fullscreen



Appendix B: VBA functions for static solution of propped cantilever beam subjected to combined transverse and axial loading

Listing of source code for VBA functions

```
Option Explicit
```

```
'=====
```

```
Function vx(T, W, E, I, L, x) As Double
```

```
' Deflection shape of the statically-indeterminate propped cantilever beam.
```

```
Dim k2, k, Lk, L2k2, Twok2, Twok, eLk, e2Lk As Double
```

```
Dim LkFac, ekx, emkx, WonT As Double
```

```
Dim a, b, c, d As Double
```

```
If T = 0 Then
```

```
    vx = -W / (48 * E * I) * (3 * L ^ 2 * x ^ 2 - 5 * L * x ^ 3 + 2 * x ^ 4)
```

```
Else
```

```
    WonT = W / T
```

```
    k2 = T / (E * I)
```

```
    k = Sqr(k2)
```

```
    Lk = L * k
```

```
    L2k2 = Lk * Lk
```

```
    Twok2 = 2 * k2
```

```
    Twok = 2 * k
```

```
    eLk = Exp(Lk)
```

```
    e2Lk = Exp(2 * Lk)
```

```
    LkFac = Lk * e2Lk + Lk - e2Lk + 1
```

```
    a = WonT * (L2k2 - 2 * Lk * eLk + 2 * eLk - 2) / (Twok2 * LkFac)
```

```
    b = -WonT * (L2k2 * eLk + 2 * Lk - 2 * eLk + 2) * eLk / (Twok2 * LkFac)
```

```
    c = -WonT * (L2k2 * e2Lk + L2k2 - 2 * e2Lk + 4 * eLk - 2) / (Twok * LkFac)
```

```
    d = -WonT * (-L2k2 * (e2Lk - 1) - 4 * Lk * eLk + 2 * e2Lk - 2) / (Twok2 * LkFac)
```

```
LkFac)
```

```
    ekx = Exp(k * x)
```

```
    emkx = Exp(-k * x)
```

```
    vx = a * ekx + b * emkx + c * x + d + WonT / 2 * x ^ 2
```

```
End If
```

```
End Function
```

```
'=====
```

```
Function dvdx(T, W, E, I, L, x) As Double
```

```
' First derivative of deflection shape with respect to x.
```

```
Dim k2, k, Lk, L2k2, Twok2, Twok, eLk, e2Lk As Double
```

```
Dim LkFac, ekx, emkx, WonT As Double
```

```
Dim a, b, c, d As Double
```

DST-Group-TR-3254

```

If T = 0 Then
  dwdx = -W / (48 * E * I) * (6 * L ^ 2 * x - 15 * L * x ^ 2 + 8 * x ^ 3)
Else
  WonT = W / T
  k2 = T / (E * I)
  k = Sqr(k2)
  Lk = L * k
  L2k2 = Lk * Lk
  Twok2 = 2 * k2
  Twok = 2 * k
  eLk = Exp(Lk)
  e2Lk = Exp(2 * Lk)
  LkFac = Lk * e2Lk + Lk - e2Lk + 1
  a = WonT * (L2k2 - 2 * Lk * eLk + 2 * eLk - 2) / (Twok2 * LkFac)
  b = -WonT * (L2k2 * eLk + 2 * Lk - 2 * eLk + 2) * eLk / (Twok2 * LkFac)
  c = -WonT * (L2k2 * e2Lk + L2k2 - 2 * e2Lk + 4 * eLk - 2) / (Twok * LkFac)
  ekx = Exp(k * x)
  emkx = Exp(-k * x)
  dwdx = k * a * ekx - k * b * emkx + c + WonT * x
End If

```

End Function

'=====

Function d2vdx2(T, W, E, I, L, x) As Double

' Second derivative of deflection shape with respect to x.

```

Dim k2, k, Lk, L2k2, Twok2, Twok, eLk, e2Lk As Double
Dim LkFac, ekx, emkx, WonT As Double
Dim a, b, c, d As Double

```

```

If T = 0 Then
  d2vdx2 = -W / (48 * E * I) * (6 * L ^ 2 - 30 * L * x + 24 * x ^ 2)
Else
  WonT = W / T
  k2 = T / (E * I)
  k = Sqr(k2)
  Lk = L * k
  L2k2 = Lk * Lk
  Twok2 = 2 * k2
  Twok = 2 * k
  eLk = Exp(Lk)
  e2Lk = Exp(2 * Lk)
  LkFac = Lk * e2Lk + Lk - e2Lk + 1
  ekx = Exp(k * x)
  emkx = Exp(-k * x)
  a = WonT * (L2k2 - 2 * Lk * eLk + 2 * eLk - 2) / (Twok2 * LkFac)
  b = -WonT * (L2k2 * eLk + 2 * Lk - 2 * eLk + 2) * eLk / (Twok2 * LkFac)
  d2vdx2 = k2 * a * ekx + k2 * b * emkx + WonT
End If

```

End Function

'=====

```

Function ThetaDeg(T, W, E, I, L, x) As Double
' Slope in degrees along the deflected shape of the beam.

Dim pi As Double

pi = 4# * Atn(1#)

ThetaDeg = dwdx(T, W, E, I, L, x) * 180 / pi

End Function

'=====

Function Nx(T, W, E, I, L, x) As Double
' Shear force distribution along beam.

Dim k2, k, Lk, L2k2, Twok2, Twok, eLk, e2Lk As Double
Dim LkFac, ekx, emkx, WonT As Double
Dim c As Double

If T = 0 Then
  Nx = (5 * L / 8 - x) * W
Else
  WonT = W / T
  k2 = T / (E * I)
  k = Sqr(k2)
  Lk = L * k
  L2k2 = Lk * Lk
  Twok2 = 2 * k2
  Twok = 2 * k
  eLk = Exp(Lk)
  e2Lk = Exp(2 * Lk)
  LkFac = Lk * e2Lk + Lk - e2Lk + 1
  c = -WonT * (L2k2 * e2Lk + L2k2 - 2 * e2Lk + 4 * eLk - 2) / (Twok * LkFac)
  Nx = -W * x - c * T
End If

End Function

'=====

Function Mx(T, W, E, I, L, x As Double) As Double
' Moment distribution along beam.

Mx = E * I * d2vdx2(T, W, E, I, L, x)

End Function

'=====

Function xdwdx0_bisect(T, W, E, I, L) As Double

```

UNCLASSIFIED

DST-Group-TR-3254

' Determine the location of the peak deflection using the bisection method.

Dim tol, xo, x1, x2, xm, dvdxx1, dvdxxm As Double
Dim n As Integer

n = 0

x1 = 0.01 * L
x2 = 0.99 * L

tol = L * 0.00000001
xo = x1

Do

 n = n + 1
 xm = (x1 + x2) / 2
 If Abs(xm - xo) < tol Then
 Exit Do
 End If
 xo = xm
 dvdxx1 = dvd(x, T, W, E, I, L, x1)
 dvdxxm = dvd(x, T, W, E, I, L, xm)
 If dvdxx1 * dvdxxm > 0 Then
 x1 = xm
 Else
 x2 = xm
 End If

Loop

xdvdx0_bisect = xm

End Function

'=====

Function vxmax(T, W, E, I, L) As Double

' Maximum deflection.

Dim xvxmax As Double

If T = 0 Then

 vxmax = (39 + 55 * Sqr(33)) / (65536 * E * I) * W * L ^ 4

Else

 xvxmax = xdvdx0_bisect(T, W, E, I, L)

 vxmax = -vx(T, W, E, I, L, xvxmax)

End If

End Function

'=====

Function xvxmax(T, W, E, I, L) As Double

' Location of the maximum deflection.

UNCLASSIFIED

```

If T = 0 Then
    xvxmax = (15 - Sqr(33)) / 16 * L
Else
    xvxmax = xdvdX0_bisect(T, W, E, I, L)
End If

End Function

'=====

Function ReactionRp(T, W, E, I, L) As Double
' Supporting reaction force at the propped end of the beam.

If T = 0 Then
    ReactionRp = 3 / 8 * W * L
Else
    ReactionRp = -Nx(T, W, E, I, L, L)
End If

End Function

'=====

Function ReactionRe(T, W, E, I, L) As Double
' Reaction force at the encastre end of the beam.

If T = 0 Then
    ReactionRe = 5 / 8 * W * L
Else
    ReactionRe = W * L - ReactionRp(T, W, E, I, L)
End If

End Function

'=====

Function ReactionMe(T, W, E, I, L) As Double
' Reaction moment at the encastre end of the beam.

If T = 0 Then
    ReactionMe = 1 / 8 * W * L ^ 2
Else
    ReactionMe = -Mx(T, W, E, I, L, 0)
End If

End Function

'=====

Function xdvdX0_subst(T, W, E, I, L) As Double
' Determine the location of the maximum deflection using substitution method.

```

UNCLASSIFIED

DST-Group-TR-3254

```

Dim k2, k, Lk, L2k2, Twok2, Twok, eLk, e2Lk As Double
Dim LkFac, ekx, emkx, WonT As Double
Dim a, b, c, d As Double
Dim xi, x, p As Double
Dim n As Integer

xi = L / 2           ' Initial guess
p = 0.00000001 * L  ' Precision
n = 0

WonT = W / T
k2 = T / (E * I)
k = Sqr(k2)
Lk = L * k
L2k2 = Lk * Lk
Twok2 = 2 * k2
Twok = 2 * k
eLk = Exp(Lk)
e2Lk = Exp(2 * Lk)
LkFac = Lk * e2Lk + Lk - e2Lk + 1

a = -WonT * (L2k2 - 2 * Lk * eLk + 2 * eLk - 2) / (Twok2 * LkFac)
b = WonT * (L2k2 * eLk + 2 * Lk - 2 * eLk + 2) * eLk / (Twok2 * LkFac)
c = WonT * (L2k2 * e2Lk + L2k2 - 2 * e2Lk + 4 * eLk - 2) / (Twok * LkFac)

Do
  n = n + 1
  x = xi
  ekx = Exp(k * x)
  emkx = Exp(-k * x)
  xi = (k * a * ekx - k * b * emkx + c) / WonT
Loop Until Abs(x - xi) < p

xdvdx0_subst = xi

End Function

```

UNCLASSIFIED

DEFENCE SCIENCE AND TECHNOLOGY GROUP DOCUMENT CONTROL DATA				1. DLM/CAVEAT (OF DOCUMENT)	
2. TITLE Deflection and Supporting Force Analysis of a Slender Beam under Combined Transverse and Tensile Axial Loads			3. SECURITY CLASSIFICATION (FOR UNCLASSIFIED REPORTS THAT ARE LIMITED RELEASE USE (L) NEXT TO DOCUMENT CLASSIFICATION) Document (U) Title (U) Abstract (U)		
4. AUTHOR(S) Witold Waldman and Xiaobo Yu			5. CORPORATE AUTHOR Defence Science and Technology Group 506 Lorimer St Fishermans Bend Victoria 3207 Australia		
6a. DST GROUP NUMBER DST-Group-TR-3254	6b. AR NUMBER AR-016-592		6c. TYPE OF REPORT Technical Report	7. DOCUMENT DATE May 2016	
8. OBJECTIVE FOLDER ID fAV1005066	9. TASK NUMBER AIR 07/283	10. TASK SPONSOR OIC-ASI-DGTA	11. NO. OF PAGES 29	12. NO. OF REFERENCES 7	
13. DST GROUP PUBLICATIONS REPOSITORY http://dspace.dsto.defence.gov.au/dspace/			14. RELEASE AUTHORITY Chief, Aerospace Division		
15. SECONDARY RELEASE STATEMENT OF THIS DOCUMENT <i>Approved for public release</i> <small>OVERSEAS ENQUIRIES OUTSIDE STATED LIMITATIONS SHOULD BE REFERRED THROUGH DOCUMENT EXCHANGE, PO BOX 1500, EDINBURGH, SA 5111</small>					
16. DELIBERATE ANNOUNCEMENT No Limitations					
17. CITATION IN OTHER DOCUMENTS Yes					
18. RESEARCH LIBRARY THESAURUS Beam theory, slender beam, propped cantilever beam, bisection method, modal analysis, flexural vibration, natural frequency					
19. ABSTRACT This report describes the deflection and supporting force analysis of a static pressure pipe that is to be used in the Defence Science and Technology Group Transonic Wind Tunnel test facility. The static pressure pipe was modelled as a slender propped cantilever beam (fixed at one end and roller-supported at the other) that is subjected to combined transverse and tensile axial loading. An analytical solution to this problem has been derived from first principles using Euler-Bernoulli beam theory, and a closed-form expression for the beam deflection as a function of the axial tension load is provided. The analytical solution was checked by performing a separate nonlinear finite element analysis using beam elements. The value of the peak deflection and its position along the beam axis was determined as a function of the applied axial tension load by solving a nonlinear equation using the bisection method. The analytical functions and numerical solution methods described in this report have been implemented for general use in a spreadsheet, and the source code for these is provided. They can be used to study other slender beam configurations that may be of interest. A modal finite element analysis of a further idealised beam configuration was also conducted to provide estimates of the natural frequencies and associated mode shapes for the beam.					